# Supporting Information

## Reproducible, stable and fast electrochemical activity from easy to make graphene on copper electrodes

Concha Bosch-Navarro,[*,a,b] Zachary P. L. Laker,[a] Neil R. Wilson,[a] Jonathan P. Rourke[b]

[a] *Department of Physics, University of Warwick, Coventry, CV4 7AL, UK*

[b] *Department of Chemistry, University of Warwick, Coventry, CV4 7AL, UK*

**Table of contents**

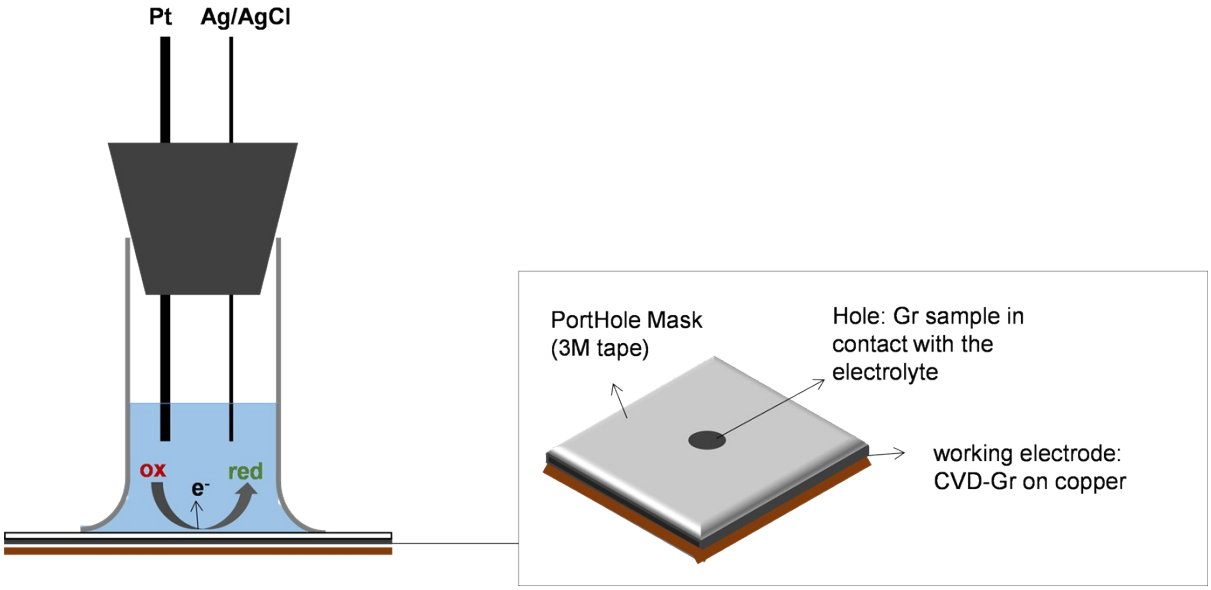


SI 1. Schematic representation of the experimental set-up for measuring the electrochemistry of CVD-Gr on copper

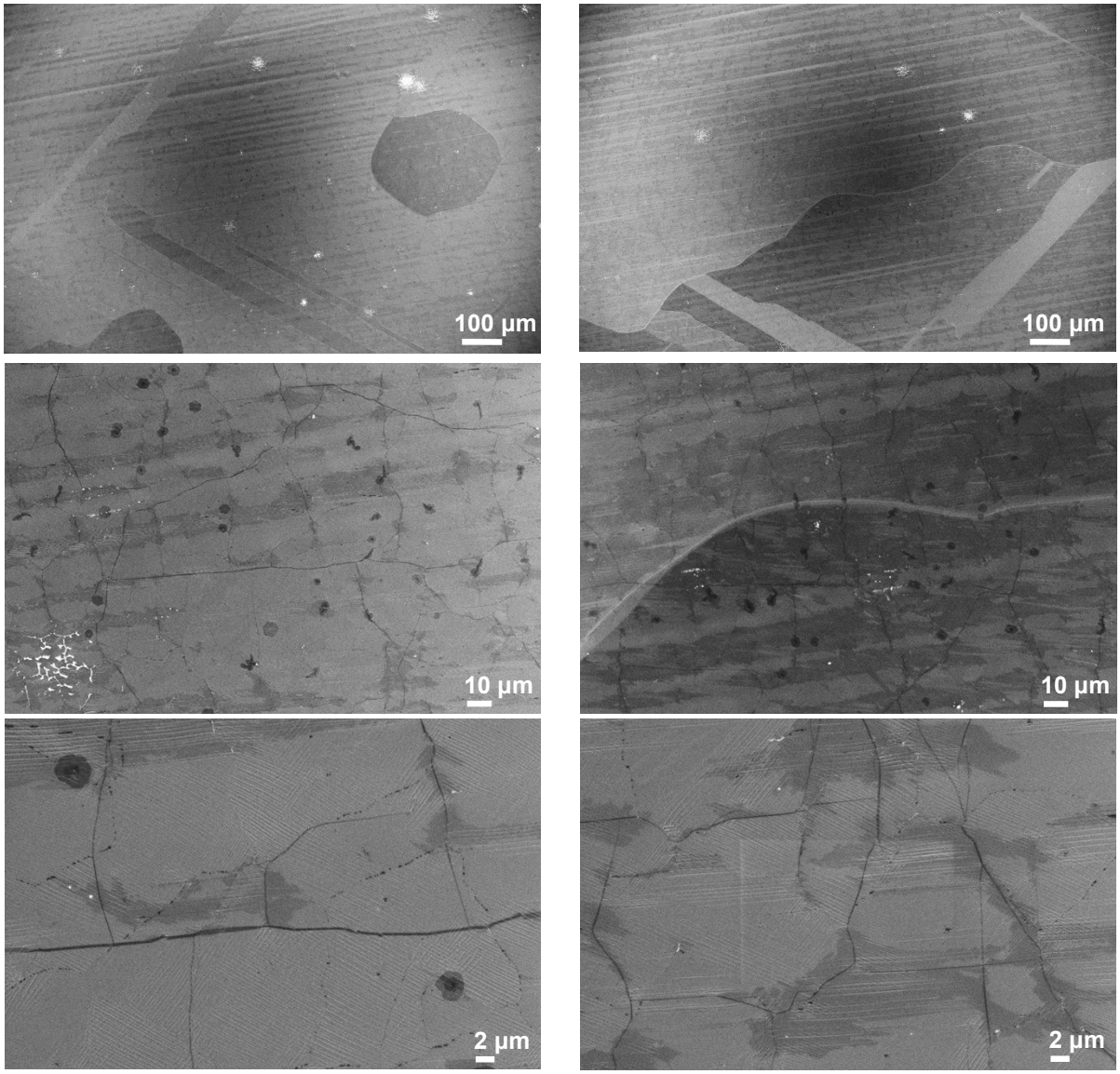


SI 2. Additional SEM images of CVD-Gr on copper.

SEM images were analysed by ImageJ.[1] The contrast difference between exposed copper regions, monolayer graphene and bilayer graphene allows the different regions to be identified by thresholding the images (see the example below in SI3) which allows rapid and robust quantification of the percentage coverage and percentage of the graphene regions that are bilayer/multilayer. ImageJ was also used to quantify the graphene island sizes for the discontinuous sheets and the density of wrinkles for the continuous graphene layers. Several images were analysed for each sample, and comparison with low magnification images were made to ensure that the results were representative.

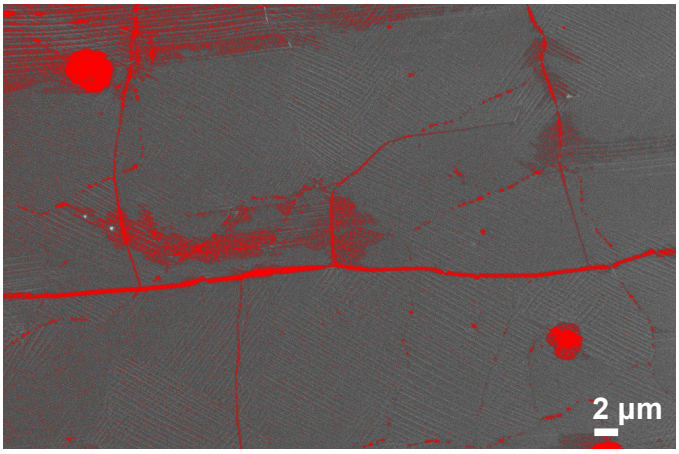


SI3. SEM image of a CVDGr in which the threshold has been modified to highlight the wrinkles and bilayer regions

[1] C.A. Schneider, W.S. Rasband and K.W. Eliceiri, *Nature Methods,* 2012, **9**, 671-675

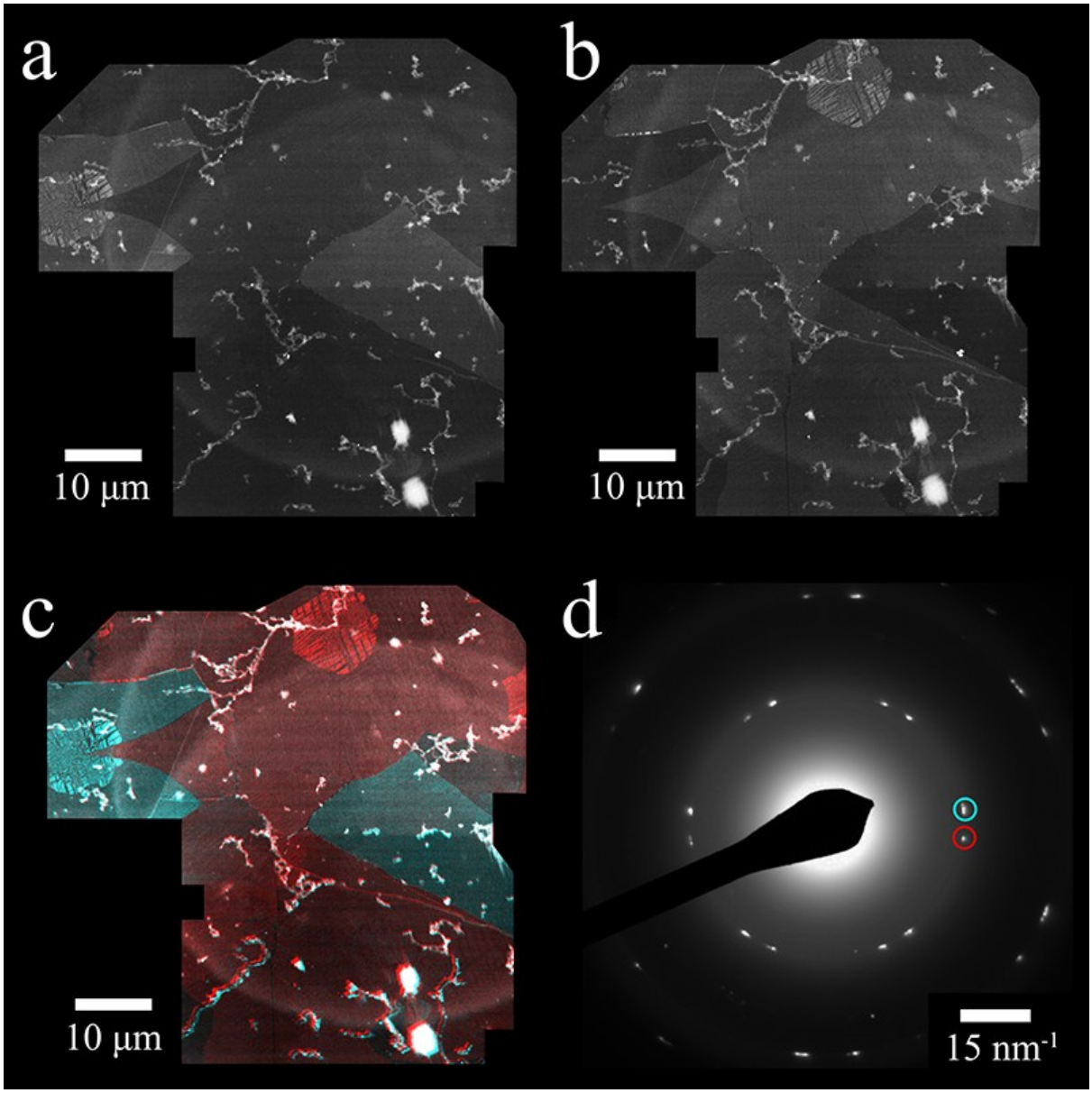


SI 4. Dark-Field TEM images of CVD-Gr and corresponding diffraction pattern indicating the size of graphtitic domains. a) Dark field image 1 corresponding to blue set of diffraction spots in d). b) Dark field image 2 corresponding to red set of diffraction spots in d). c) Composite colour map of dark field images a) and b) providing a colour map of the graphitic domains present in the image. d) Diffraction pattern showing two contributing graphitic domains at different orientations, with coloured circles matching the contributing areas in c)

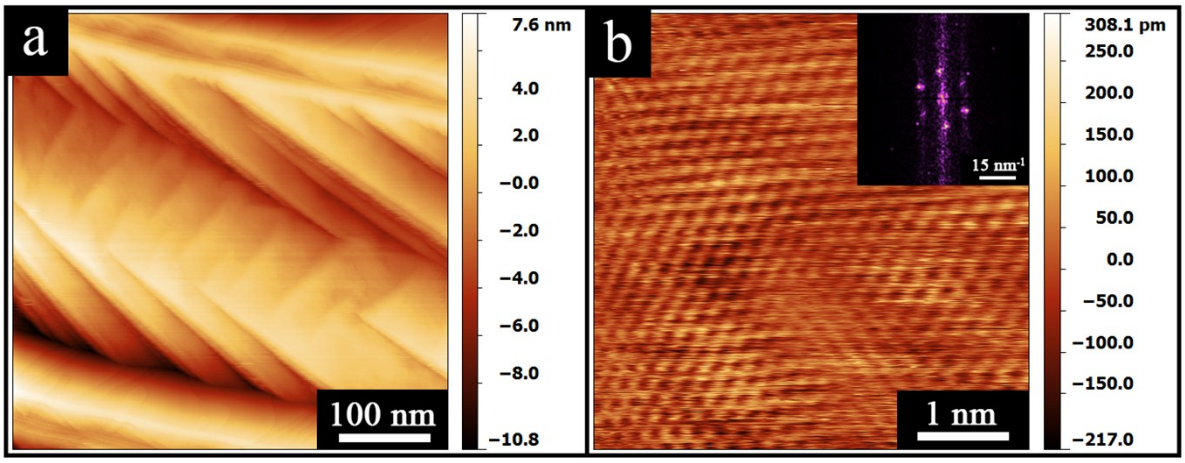


SI 5. STM images of CVD-Gr on copper. The lower magnification image in (a) shows that the graphene follows the copper surface (atomic steps and facets in the underlying surface can be seen), is defect free, and is perfectly clean over large areas. (b) The higher magnification image clearly shows the honeycomb lattice structure of graphene, with the inset FFT corresponding well with the reciprocal lattice structure of graphene.

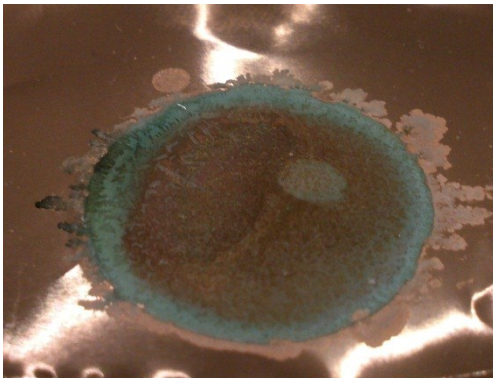

(a)

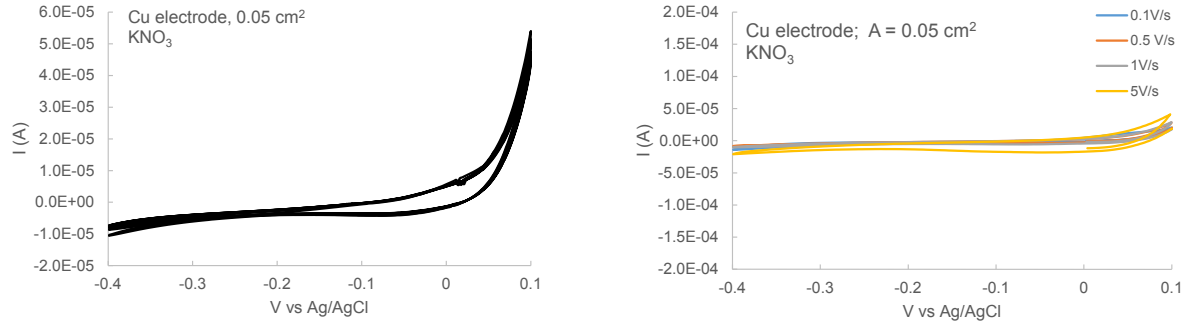


(b)

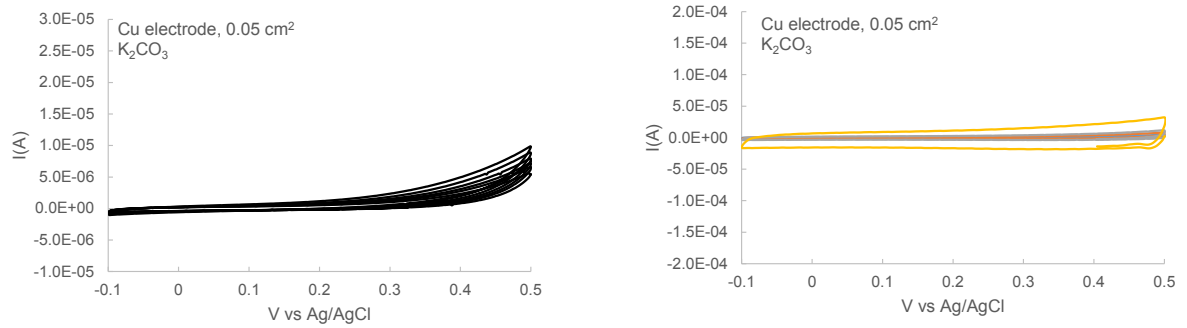


(c)

SI 6. a) Photograph of a copper foil substrate after electrochemical treatment in the presence of KCl. A green deposit corresponding to cupric hydroxide ($Cu(OH)_2$), atacamite ($Cu_2(OH)_3Cl$) and malachite ($CuCO_3$ $Cu(OH)_2$ is observed, and clearly shows the electrochemical incompatibility of Cu and KCl. In b) and c) the electrochemical behaviour of a copper foil electrode in the presence of $KNO_3$ and $K_2CO_3$ are shown. On the *left* of each figure cyclic voltammograms after 10 successive cycles are shown, while on the *right* the effect of the scan rate is studied. As shown, in the electrochemical window studied, no apparent electrochemical processes took place either in the presence of $KNO_3$ or in the presence of $K_2CO_3$, thus allowing their use as electrolytes for the analysis of electrochemical processes on copper substrates.

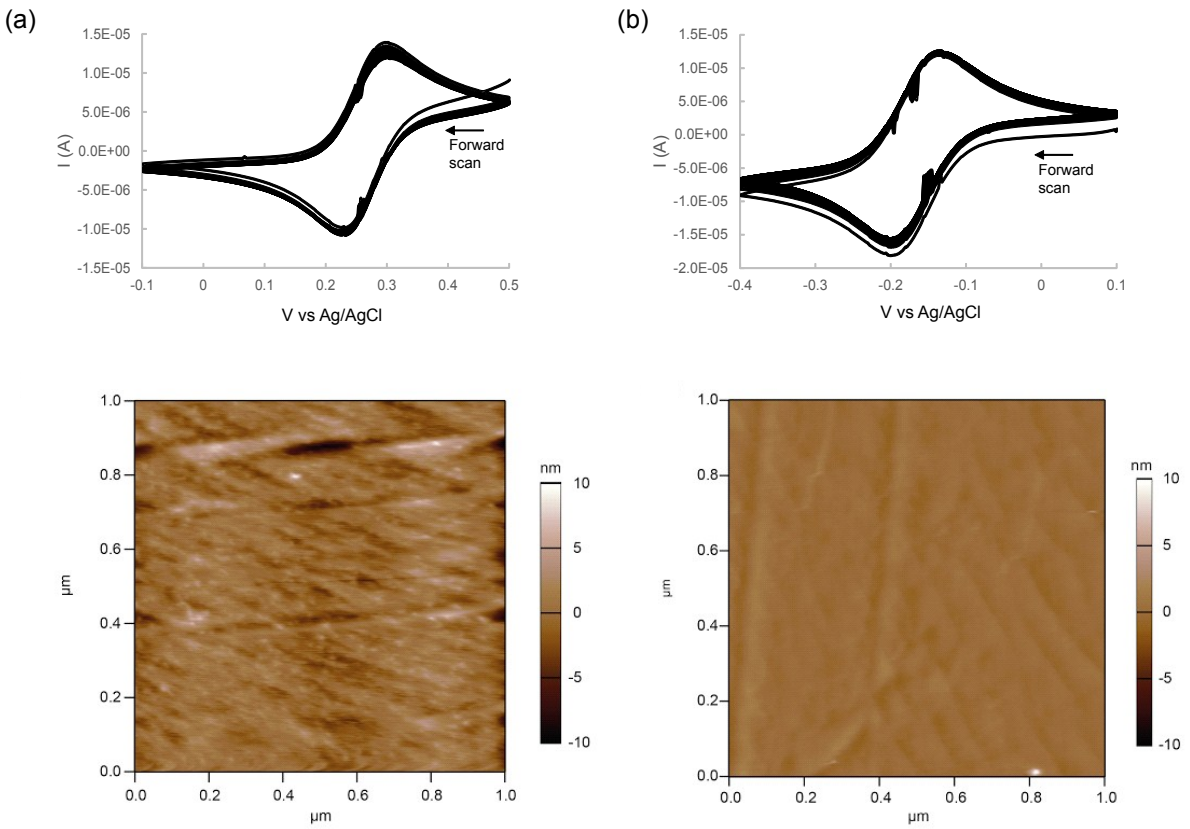


SI 7. (*top*) Cyclic voltammograms after 50 successive cycles show the great stability of the CVD-Gr on copper working electrode for both studied systems: a) 1 mM $[Fe(CN)_6]^{4-}$ in $K_2CO_3$ 0.5 M, and b) 1 mM $[Ru(NH_3)_6]^{3+}$ in 0.5 M $KNO_3$. The experiments shown have been carried out at a scan rate of 0.1 $Vs^{-1}$. (*bottom*) corresponding AFM images. As shown, the sample surface is still fairly clean with no large visible deposits observed after 50 consecutive cycles.

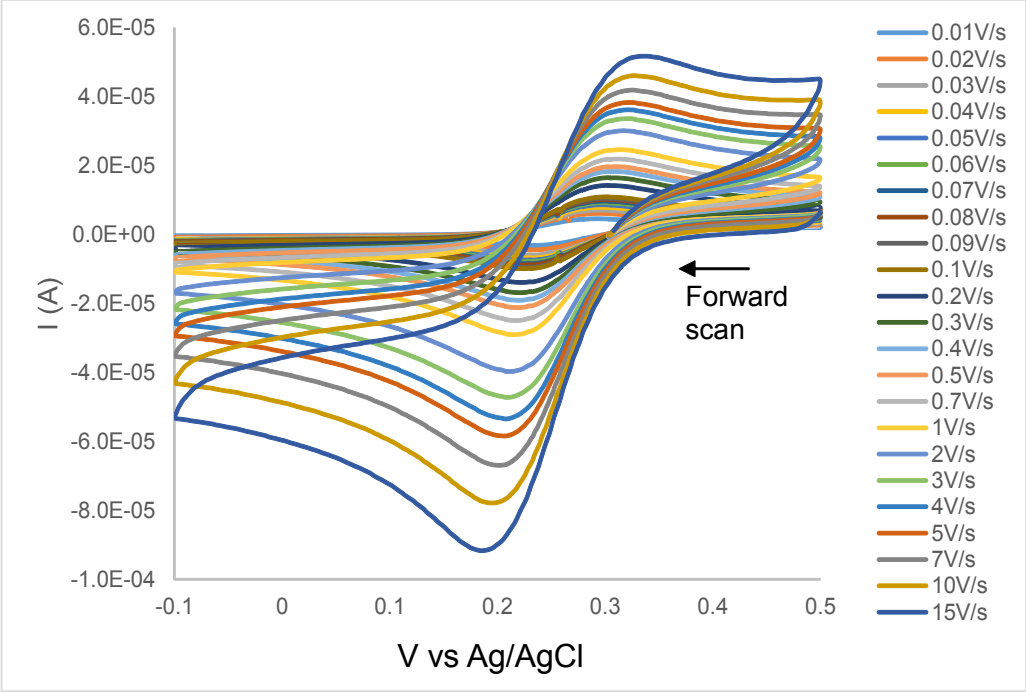


(a)

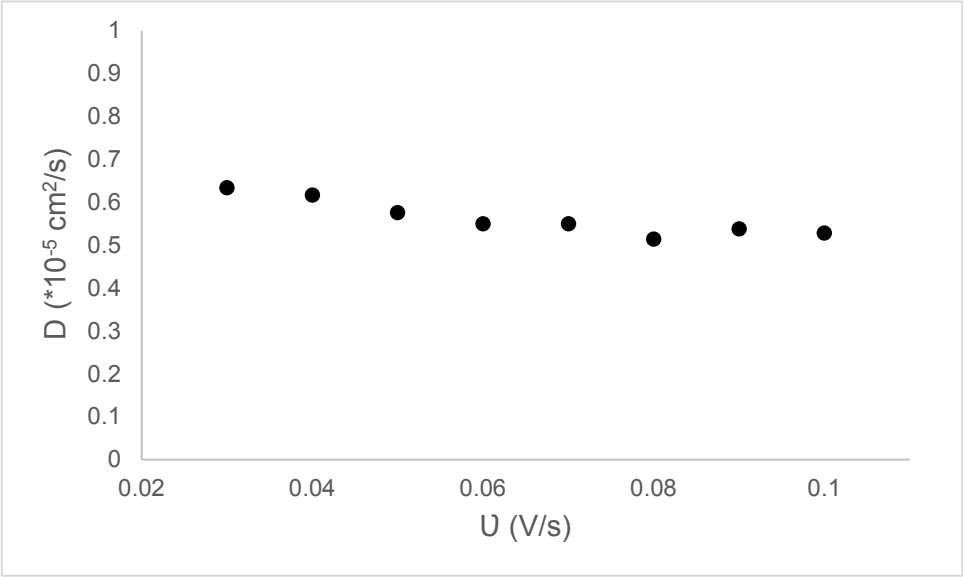


(b)

SI 8. a) Additional cyclic voltammograms for 1mM $[Fe(CN)_6]^{4-}$ in $K_2CO_3$ 0.5M when using CVD-Gr on copper as working electrode. In the figure is clearly observed the dependence of the $\Delta E_p$ with the scan rate, showing increased $\Delta E_p$ for greater scan rates. b) Values obtained for the diffusion coefficient ($D$) by applying the Randles-Sevcik equation for different scan rates. From the calculated values the diffusion coefficient can be calculated to be $D = (0.56 \pm 0.1) \times 10^{-5}$ cm$^2$ s$^{-1}$

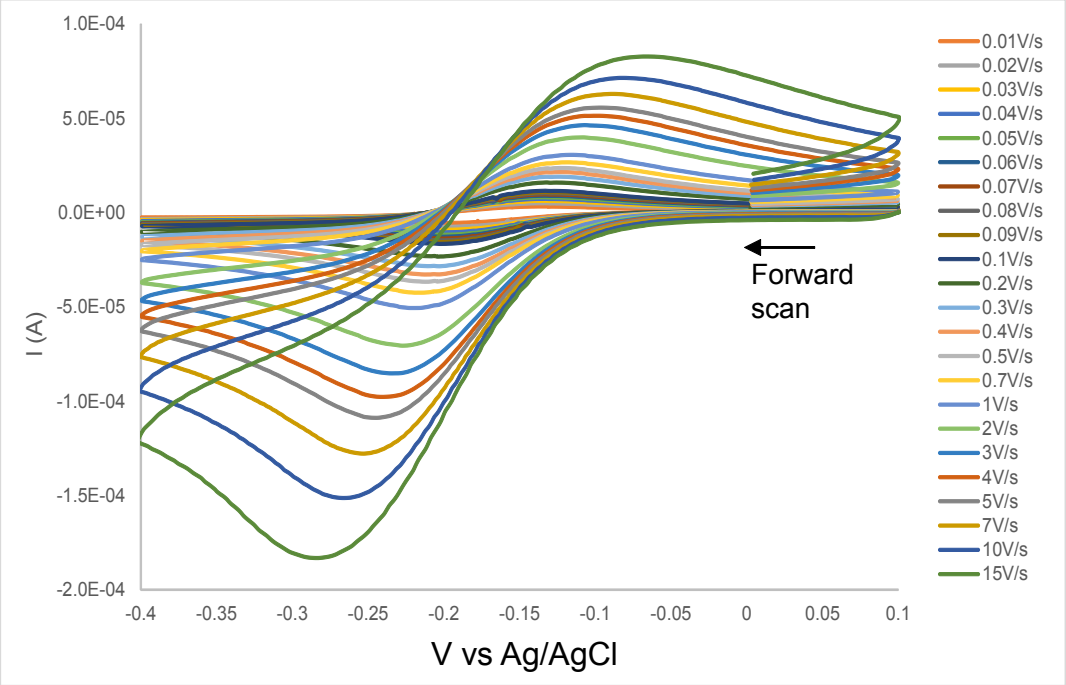


(a)

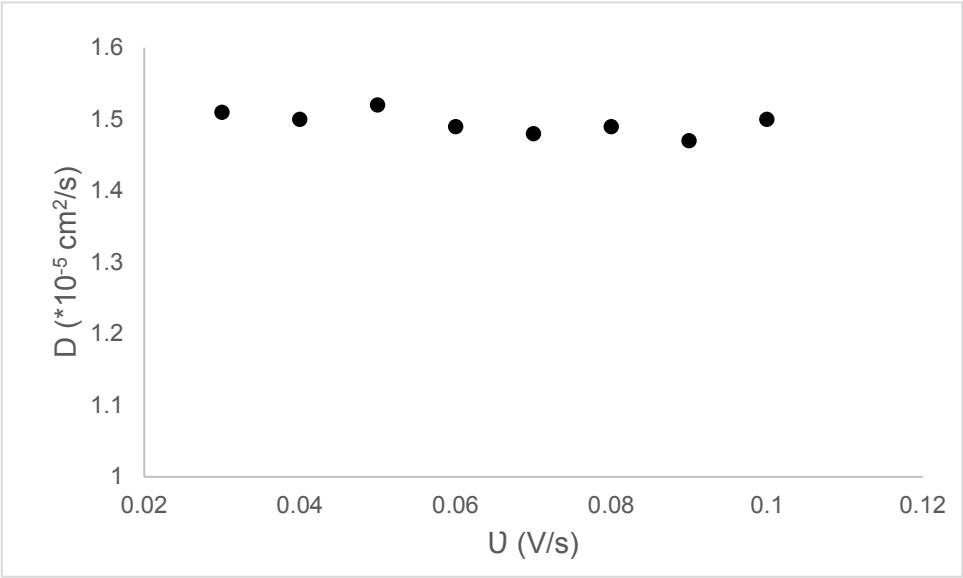


(b)

SI 9. a) Additional cyclic voltammograms for 1mM $[Ru(NH_3)_6]^{3+}$ in $KNO_3$ 0.5M when using CVD-Gr on copper as working electrode. In the figure is clearly observed the dependence of the $\Delta E_p$ with the scan rate, showing increased $\Delta E_p$ for greater scan rates. b) Values obtained for the diffusion coefficient ($D$) by applying the Randles-Sevcik equation for different scan rates. From the calculated values the diffusion coefficient can be calculated to be $D = (1.49 \pm 0.2)\ 10^{-5}\ cm^2\ s^{-1}$

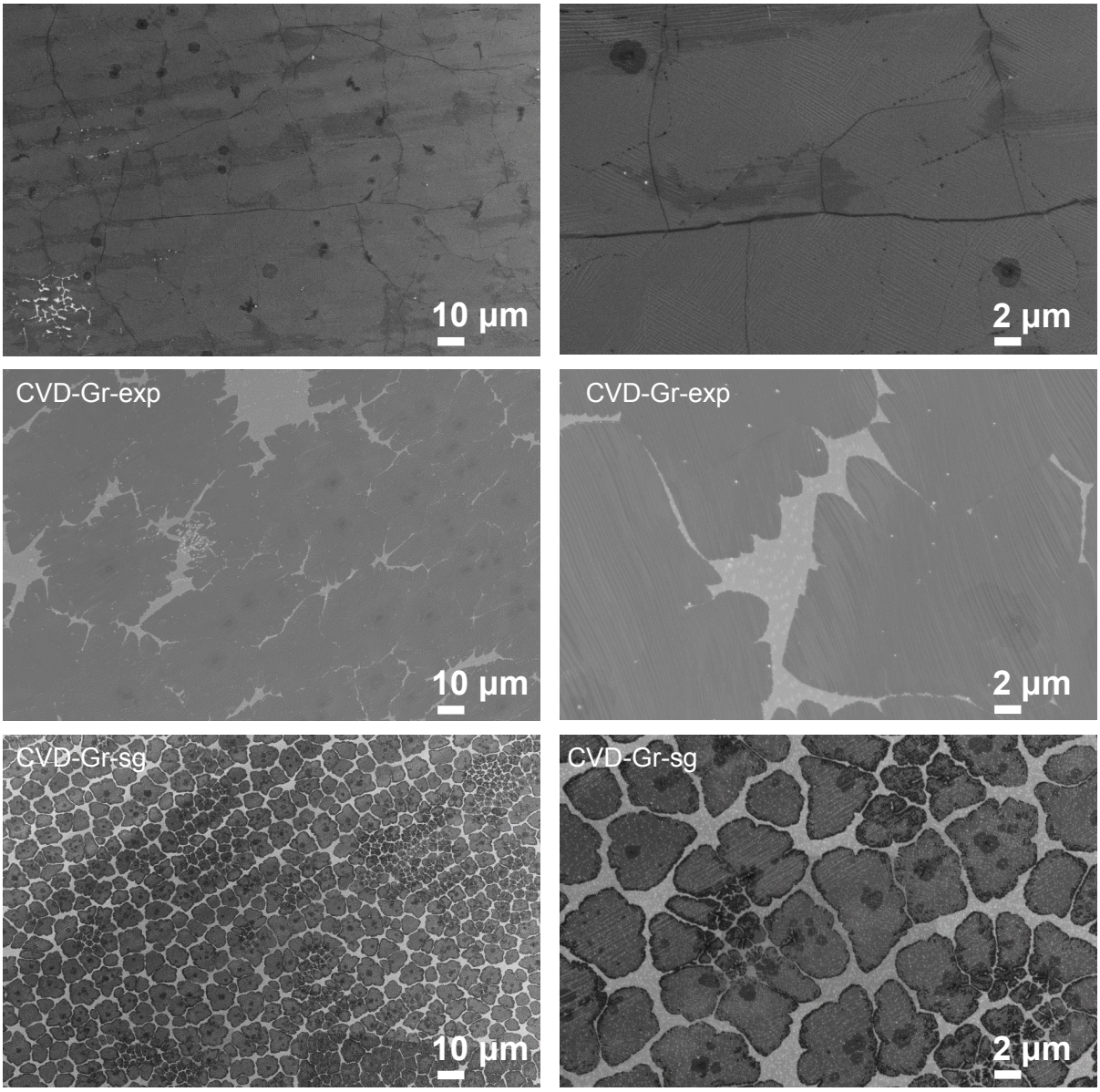


SI 10. Additional SEM images of CVD-Gr (*top*), CVD-Gr-exp (*middle*) and CVD-Gr-sg (*bottom*).

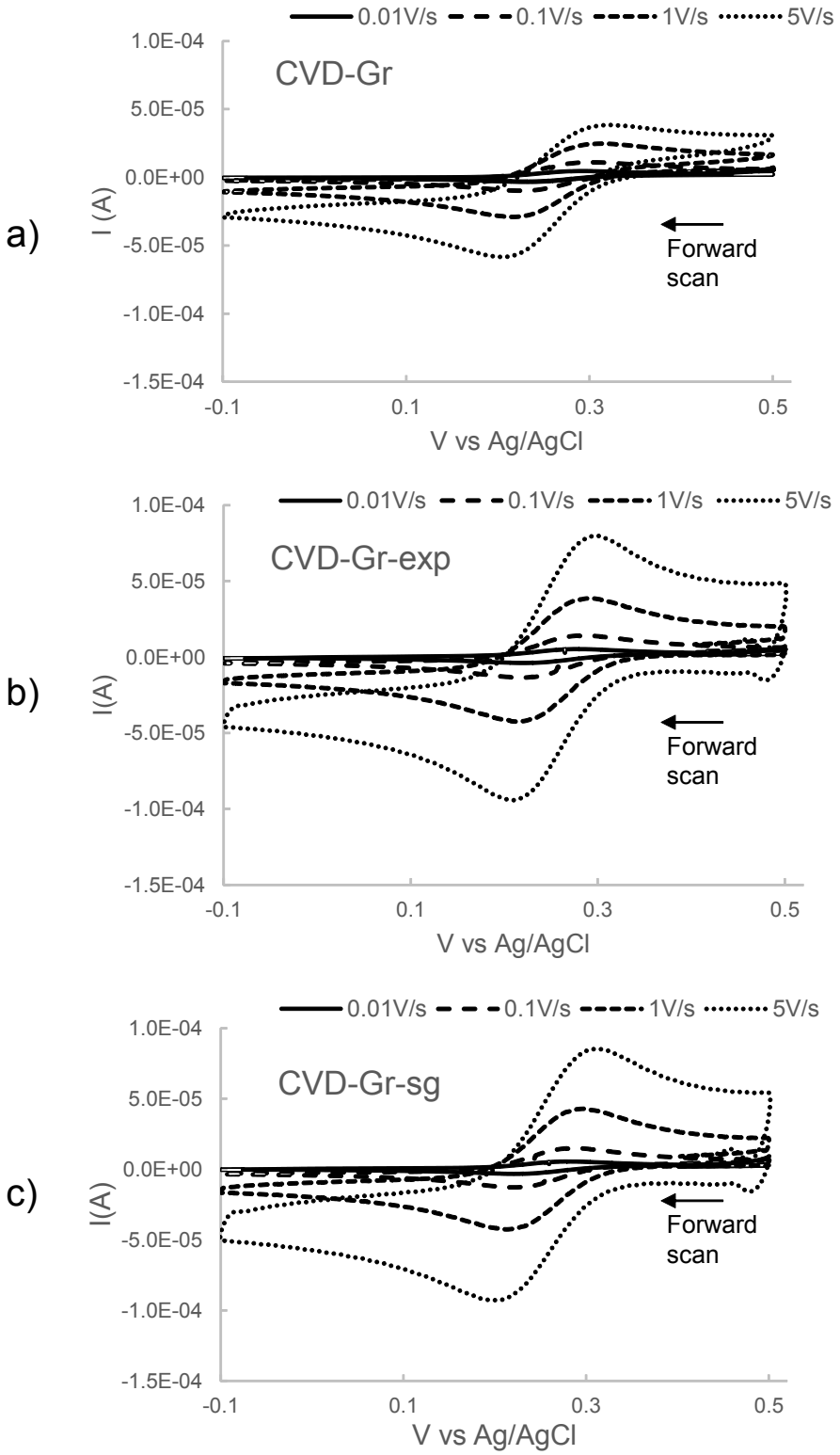


SI 11. Representative CVs recorded at 0.01 V $s^{-1}$ (solid line), 0.1 V $s^{-1}$ (dashed line), 1 V $s^{-1}$ (dotted line) and 5 V $s^{-1}$ (star-like line) against 1mM $[Fe(CN)_6]^{4-}$ in $K_2CO_3$ 0.5M obtained when using (a) CVD-Gr, (b) CVD-Gr-exp and (c) CVD-Gr-sg as working electrodes.

Table SI11. $\Delta E_p$ as extracted from the CVs shown in Figure SI 11

| $\Delta E_p$ (mV) | | | |
|---|---|---|---|
| Scan Rate | CVD-Gr | CVD-Gr-exp | CVD-Gr-sg |
| 0.01 V $s^{-1}$ | 64 ± 1 | 60 ± 1 | 57 ± 1 |
| 0.1 V $s^{-1}$ | 60 ± 1 | 60 ± 1 | 65 ± 1 |
| 1 V $s^{-1}$ | 83 ± 1 | 83 ± 1 | 89 ± 1 |
| 5 V $s^{-1}$ | 110 ± 2 | 100 ± 2 | 113 ± 2 |

'The similarity in the peak to peak separations as a function of scan rate for the different types of sample suggests that the electron transfer kinetics are similar for the $[Fe(CN)_6]^{4-}$ redox couple. This is despite the orders of magnitude changes in wrinkle density, grain size and 'edge-plane' density. This strongly suggests that here the electrochemical response is dominated by the graphene basal plane, even for the inner sphere $[Fe(CN)_6]^{4-}$ redox couple.'

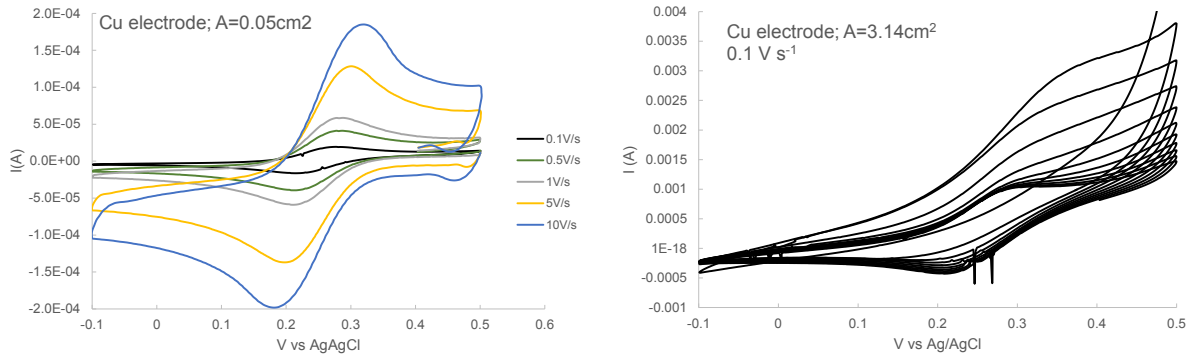


(a)

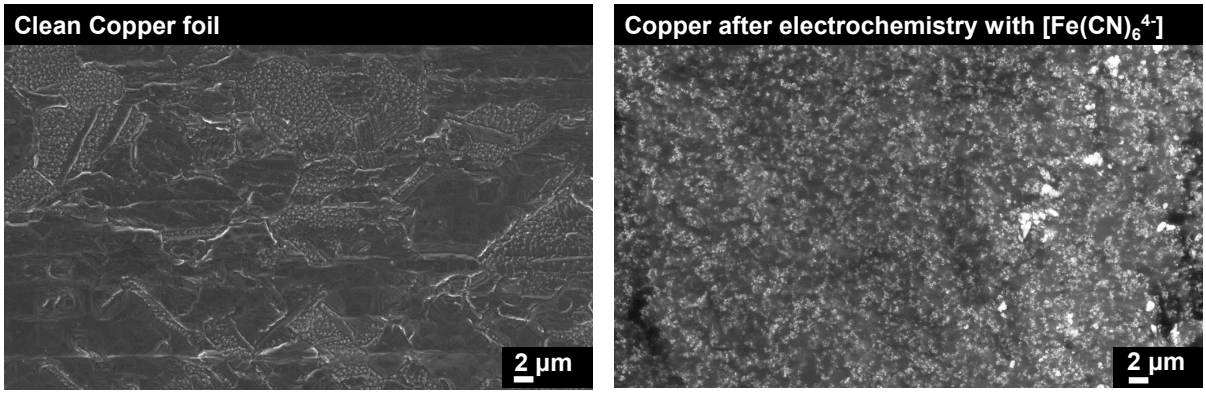


(b)

SI 12.(a) CV of copper foil against 1mM $[Fe(CN)_6]^{4-}$ in $K_2CO_3$ 0.5M performed at different scan rates (*left*) and showing 10 consecutive cycles at 0.1 V $s^{-1}$ (*right*). Note that the difference in the peak current values between the two graphs is due to the difference in the electrode areas. The electrode having an area of 3.14 $cm^2$ was further analysed by SEM as shown in (b). For comparison, SEM of clean copper foil is also included.

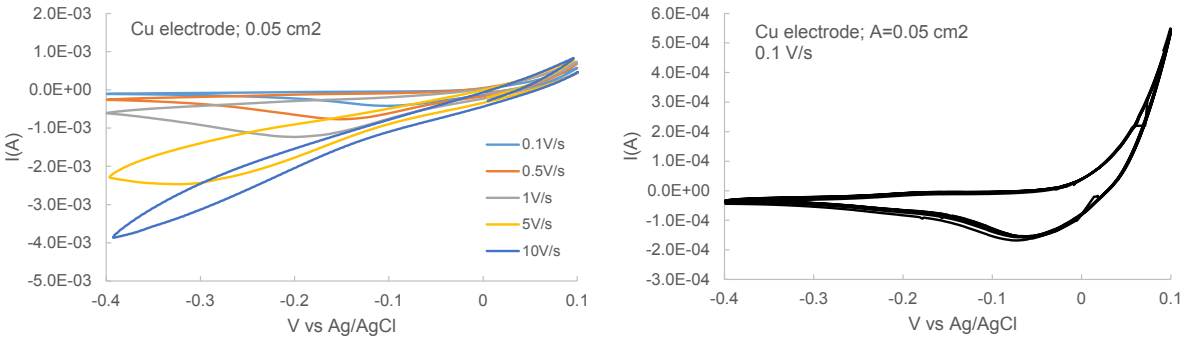


SI 13. CV of copper foil against 1mM $[Ru(NH_3)_6]^{3+}$ in 0.5M $KNO_3$ performed at different scan rates (*left*) and showing 10 consecutive cycles at 0.1 V $s^{-1}$ (*right*).

The absence of redox peaks during the electrochemical analysis of a clean copper foil against $[Ru(NH_3)_6]^{3+}$ confirms the negligible effect that the supporting copper has in the electrochemical signal measured for CVD-Gr (Figure 4 of main text). Moreover, in contrast to the changing behaviour shown by the copper electrode against $[Fe(CN)_6]^{4-}$ during successive cycles (Figure S111), the electrochemical signal of the copper electrode against $[Ru(NH_3)_6]^{3+}$ remains constant, which rules out that any adsorption is taking place.